Topologically Protected and Conventional Subbands in a 1T'-MoS2 Nanoribbon Channel

Viktor Sverdlov
Christian Doppler Laboratory for Nonvolatile Magnetoresistive Memory and Logic at the Insitute for Microelectronics, Technische Universität Wien
Vienna, Austria
sverdlov@iue.tuwien.ac.at

Al-Moatasem Bellah El-Sayed
Institute for Microelectronics Technische Universität Wien
Vienna, Austria
el-sayed@iue.tuwien.ac.at

Hans Kosina
Institute for Microelectronics Technische Universität Wien
Vienna, Austria
kosina@iue.tuwien.ac.at

Siegfried Selberherr
Institute for Microelectronics Technische Universität Wien
Vienna, Austria
Selberherr@TUWien.ac.at

2020 Joint International EUROSOI Workshop and International Conference on Ultimate Integration on Silicon (EUROSOI-ULIS) | 978-1-7281-8765-5/20/$31.00 ©2020 IEEE | DOI: 10.1109/EUROSOI-ULIS49407.2020.9365289

***Abstract*—Continuous miniaturization brought the feature size of silicon technology into the nanometer scale, where performance enhancement cannot be easily achieved by further feature size reduction. The use of new materials with advanced properties has become mandatory to meet the needs for higher performance at reduced power. Topological insulators possess highly conductive topologically protected edge states insensitive to scattering and thus suitable for energy efficient high speed devices. Here, we evaluate the subband structure in a nanoribbon of 1T'-MoS_2 by applying an effective k·p Hamiltonian in a confined geometry.**

Keywords—topological insulators, topologically protected edge states, nanoribbons, subbands, k.p Hamiltonian

I. Introduction

Topological insulators (TIs) belong to a new class of semiconducting materials with highly conductive edge states. These edge states lie in the band gap of the bulk insulating material. In order to have states in the gap, the bulk host material must possess an inverted band structure with the valence band edge lying above the conduction band edge. The standard band order is restored at the edge, where the host material is interfaced with a normal dielectric (air). The edge states then possess a linear Dirac-like energy dispersion. The edge states are topologically protected by time-reversal symmetry, which results in electron propagation without backscattering. This property makes them attractive as a material for highly conductive transistor channels.

Recent progress in fabrication and investigation of two-dimensional (2D) TIs [1] demonstrates the potential of these materials for use in advanced microelectronics. Having highly conductive channels is not sufficient to make a good transistor switch as one has to have a possibility to suppress the current through the channel. A plausible option is to close the gap in the host bulk material. In this case scattering between the protected edge and the non-protected electron-hole bulk states results in strong scattering which effectively reduces the current through the edge states [2]. When the normal gap in the bulk material is created by restoring the order of the bands, there are no edge states possible in the gap, and the current due to these states is absent. Therefore, an ability to modulate the gap and the gap nature by changing an external parameter (an electric field or gate voltage) opens a path to a current switch, where the current carrying topologically protected states either exist in the gap or not [2].

II. Method

Recently it was discovered that, if the well-known 2D material MoS_2 which has a high promise for future microelectronic devices [3], is grown in a 1T' phase, it becomes a TI [4]. The inverted band structure is well described by parabolic dispersion relations, where $\mathbf{k} = (k_x, k_y)$ is the wave vector, $E_p(k_x,k_y)$ and $E_d(k_x,k_y)$ refer to the valence and conduction bands, respectively, and $m_{y(x)}^{d(p)}$ denote the effective masses [4]:

$$E_p(k_x,k_y) = \delta - \frac{\hbar^2 k_y^2}{2m_y^p} - \frac{\hbar^2 k_x^2}{2m_x^p} \tag{1}$$

$$E_d(k_x,k_y) = -\delta + \frac{\hbar^2 k_y^2}{2m_y^d} + \frac{\hbar^2 k_x^2}{2m_x^d} \tag{2}$$

These bands intersect at $k_y = \pm k_0$, where

$$k_0 = \sqrt{\frac{4\delta}{\hbar^2}\frac{m_y^d m_y^p}{m_y^d + m_y^p}}\ . \tag{3}$$

Therefore, without spin-orbit interaction, the material would be a semi-metal. The spin-orbit interaction makes the conduction and the valence bands to interact, which opens gaps around the intersection points. The effective Hamiltonian **H** can be written as [4]

$$\mathbf{H}(\mathbf{k}) = \begin{pmatrix} E_p(k_x,k_y) & 0 & -iv_1\hbar k_x & v_2\hbar k_y - \alpha E_z \\ 0 & E_p(k_x,k_y) & v_2\hbar k_y - \alpha E_z & -iv_1\hbar k_x \\ iv_1\hbar k_x & v_2\hbar k_y - \alpha E_z & E_d(k_x,k_y) & 0 \\ v_2\hbar k_y - \alpha E_z & iv_1\hbar k_x & 0 & E_d(k_x,k_y) \end{pmatrix}. \tag{4}$$

Here $v_{1(2)}$ are the velocities defining the strength of the spin-orbit interaction and αE_z describes the additional Rashba splitting between the bands due to the perpendicular vertical electric field E [4,5]. E_z is able to manipulate and to change the nature of the gaps close to the degeneracy points at $k_y = \pm k_0$. The parameters [4] are listed in Table 1. It is convenient to perform a canonical transformation of the Hamiltonian (4) by means of the two unitary matrices **A** and **B** as

$$\boldsymbol{H'}(\mathbf{k}) = \mathbf{B^{-1}}\,\mathbf{A^{-1}}\mathbf{HAB}, \tag{5}$$

where the matrices **A** and **B** have the following structure:

$$\mathbf{A} = \frac{1}{2}\begin{pmatrix} 1 & 1 & 1 & 1 \\ 1 & 1 & -1 & -1 \\ 1 & -1 & 1 & -1 \\ 1 & -1 & -1 & 1 \end{pmatrix} \tag{6}$$

TABLE I.

Variable	Value
2 δ	0.66 eV
$\boldsymbol{v_1}$	3.87 10^5 m/s
$\boldsymbol{v_2}$	0.46 10^5 m/s
$\boldsymbol{m_x^p}$	0.5 $\boldsymbol{m_e}$
$\boldsymbol{m_y^p}$	0.16 $\boldsymbol{m_e}$
$\boldsymbol{m_x^d}$	2.48 $\boldsymbol{m_e}$
$\boldsymbol{m_y^d}$	0.37 $\boldsymbol{m_e}$
$\boldsymbol{\alpha}$	0.03 *e* nm
$\boldsymbol{k_0}$	1.485 nm^{-1}
d	$40\boldsymbol{k_0^{-1}} = \boldsymbol{26.93}$ **nm**

Table 1 Parameters [4,5] used in the model. m_e is the electron mass, *e* is the electron charge, and *d* is the width in OY direction.

$$\mathbf{B} = \frac{1}{\sqrt{2}}\begin{pmatrix} 1 & 1 & 0 & 0 \\ -1 & 1 & 0 & 0 \\ 0 & 0 & 1 & 1 \\ 0 & 0 & -1 & 1 \end{pmatrix} \tag{7}$$

After the unitary transformation the Hamiltonian $\boldsymbol{H'}$ is in the block-diagonal form

$$\boldsymbol{H'} = \begin{pmatrix} H(\mathbf{k}) & 0 \\ 0 & H^{+}(-\mathbf{k}) \end{pmatrix}, \tag{8}$$

where (Z^+) stands for a conjugate transpose matrix Z. The 2×2 Hamiltonian $H(\mathbf{k})$ possesses the following structure:

$$H(\mathbf{k}) = \begin{pmatrix} \delta - \frac{\hbar^2 k_y^2}{2m_y^p} - \frac{\hbar^2 k_x^2}{2m_x^p} & v_2 k_y - \alpha E_z + i\, v_1 k_x \\ v_2 k_y - \alpha E_z - i\, v_1 k_x & -\delta + \frac{\hbar^2 k_y^2}{m_y^d} + \frac{\hbar^2 k_x^2}{m_x^d} \end{pmatrix} \tag{9}$$

The possibility to express the Hamiltonian in the form (8) is a consequence of the time-reversal symmetry. It then follows that, if allowed, at every edge there are two topologically protected modes propagating in opposite directions with opposite spins. As the spin-down wave function $\Psi_\downarrow(k_x,y)$ of the lower 2×2 block $H^*(-\mathbf{k})$ can be easily found from the spin-up solution for the upper block as $\Psi_\downarrow(k_x, y) = -i\sigma_y \Psi_\uparrow^*(k_x, y)$ [6], where σ_y is the Pauli matrix, we will be only focusing on the 2×2 block Hamiltonian $H(\mathbf{k})$.

If we measure energies in units of $E_0 = 2\,\delta$ and the wave vectors $\mathbf{k} = (k_x, k_y)$ in units of k_0, the Hamiltonian (9) can be conveniently written in the dimensionless form

$$H(\mathbf{k}) = \begin{pmatrix} \frac{1}{2} - k_y^2 \frac{m}{m_y^p} - k_x^2 \frac{m}{m_x^p} & v_2 k_y - \alpha E_z + i\, v_1 k_x \\ v_2 k_y - \alpha E_z - i\, v_1 k_x & -\frac{1}{2} + k_y^2 \frac{m}{m_y^d} + k_x^2 \frac{m}{m_x^d} \end{pmatrix}, \tag{10}$$

where $m = \frac{m_y^d m_y^p}{m_y^d + m_y^p}$ and $v_{1(2)}$ are the dimensionless velocities.

The energy dispersion obtained from (10) with an offset of $\Delta E = \frac{1}{2}\frac{m_y^d - m_y^p}{m_y^d + m_y^p}$ is shown in Fig.1 for k_x=0. If the off-diagonal terms in (10) is zero, the dispersion curves intersect at $k_y = \pm k_0$

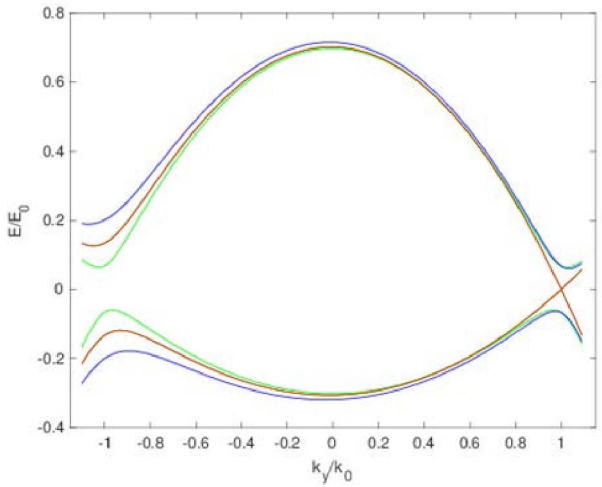

Fig.1 Bulk energy dispersion in 1T'-MoS_2 two-dimensional material, k_x=0. Green dispersion displays the gaps at $k_y = k_0$ in the inverted band structure at E_z=0. Increasing the electric field to $E_z = v_2$ closes the gap (red curve) and reopens it again as a direct gap ($E_z = 2v_2$, blue curve).

and E_z=0. The spin-orbit interaction described by the off-diagonal terms opens a gap at the intersection of the valence and conduction at $k_y = \pm k_0$., (Fig.1, green line). The gap also depends on k_x which enters in the off-diagonal in a similar way to k_y.

By applying an electric field E_z along the OZ axis the gap at one of the minima can be reduced, completely closed (Fig.1, red line), or even opened again (Fig.1, blue line) at large electric fields. The gap at large electric fields becomes direct, so no edge states are allowed within the bulk gap.

III. Quantzation in a Nanoribbon

We consider a nanoribbon with the width in OY direction of $d = 40/k_0$. In this case, only quantized values of the momentum k_y along the quantization axis OY perpendicular to the nanoribbon are allowed. In addition, it is expected that at E_z =0 two topologically protected highly conductive edge states localized at opposite interfaces of a nanoribbon must exist within the gap opened by the spin-orbit interaction in the inverted band structure at $k_y = \pm k_0$ (Fig.1, green line).

Let us outline how we obtain the subband structure. A line drawn at any fixed energy *E* outside of the spin-orbit gap crosses the dispersion curve in Fig.1 at four distinct k_y points: k_j, j=1,…,4 Therefore, a general form of the subband wave function $\psi_{k_x}(y)$ in the quantization OY direction is written as

$$\psi_{k_x}(y) = \sum_{j=1}^{4} A_j \begin{pmatrix} 1 \\ a(k_j, E) \end{pmatrix} \exp(ik_j y), \tag{11}$$

where A_j (j=1,...,4) are four constants and

$$a(k_j, E) = \frac{-\frac{1}{2} + k_j^2 \frac{m}{m_y^p} + k_x^2 \frac{m}{m_x^p} + E}{v_2 k_j - \alpha E_z + i\, v_1 k_x} \tag{12}$$

The subband energies are obtained by setting the wave function to zero at both edges. The characteristic equation is solved numerically, in complete analogy to the problem of finding the eigenenergies and eigenfunctions of a 2-band **k·p** Hamiltonian in silicon films [7].

To illustrate the numerical procedure, let us introduce the matrix **M** as

$$\mathbf{M} = (M_1 \quad M_2 \quad M_3 \quad M_4) \tag{13}$$

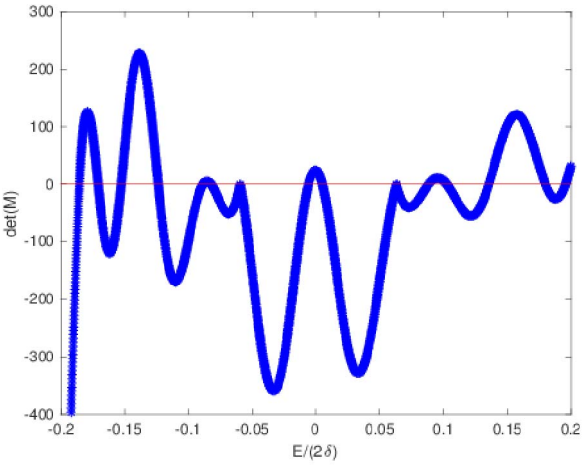

Fig.2 Real (blue) and imaginary (red) parts of det(**M**) computed at k_x =0, E_z = 0, d=40k_0^{-1}. The bulk gap is seen at at E≈ ±0.065, where the real part touches the OX axis from below. The subband energies are obtained from det(**M**)=0. Topological edge states are seen in the bulk gap (E≈ ±0.005).

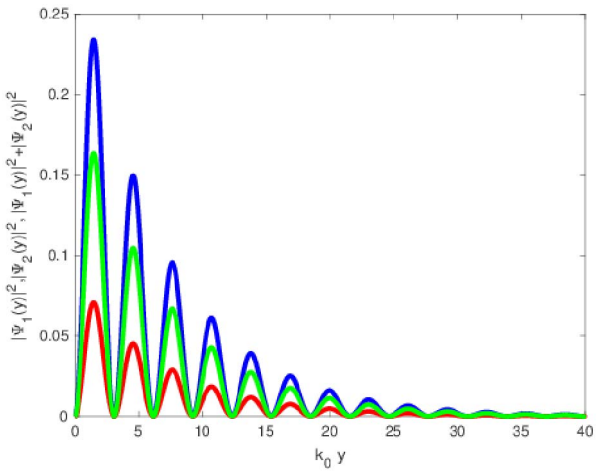

Fig.3 The wave function square (blue) and its two spinor components (green and red) of the topological edge state evaluated at $\frac{\alpha E_z}{v_2 k_0} = 0.1$ and k_x =0.1k_0. The subband wave function shows both oscillation and an exponential decay.

with the columns M_j, j=1,..,4.

$$M_j = \begin{pmatrix} 1 \\ a(k_j, E) \\ \exp(ik_j d) \\ a(k_j, E)\exp(ik_j d) \end{pmatrix} \qquad (14)$$

The boundary conditions that the wave function (11) must be zero at both edges of the nanoribbon is then written as

$$\mathbf{M}\,\mathbf{A} = 0, \qquad (15)$$

where the vector **A**=$(A_1, A_2, A_3, A_4)^{\mathrm{T}}$is made by constants in (11). Equation (15) has nontrivial solutions for **A,** if

$$\det(\mathbf{M}) = 0. \qquad (16)$$

Fig.2 displays the behaviour of the real part (the imaginary part is zero for E_z=0) of the determinant as a function of energy, for k_x=0. We are interested in the crossings of the curve with the axis OX. We easily identify the gap due to the spin-orbit interaction at E≈ ±0.065. The value of the determinant approaches the axis from negative values and touches it at a single point. Indeed, when we the constant energy line touches the minimum (maximum) of the dispersion relation shown with the green line in Fig.1, k_1= k_2 and k_3= k_4, so (16) is zero.

All other intersections with the OX axis correspond to subbands. However, we clearly observe the two roots in the gap at E≈ ±0.005 A close inspection shows that the wave vectors k_j corresponding to these solutions are not real but complex. The wave functions corresponding to these solutions in the gap are located at an edge of the nanoribbon as shown in Fig.3 for k_x =0.1k_0 and in Fig.4 for for k_x = - 0.1k_0. In contrast to [6], where only an exponential decay was predicted, the wave function (11) displays both oscillations and decay. Although the structure of the Hamiltonians considered here and in [6] are similar, the actual parameters are different. In particular, in the case considered here, the spin-orbit gaps are open at the finite values of k_y =± k_0 (Fig.1, green line). The shift of the bulk band's minima from the Gamma-point at k_y=0 is responsible for the subband wave functions displaying not only the decay but the oscillations as well. Therefore, these solutions correspond to the topologically protected edge modes, which is confirmed by the complex values of the solutions for k_j

The roots of the determinant further away from E=0 correspond to the traditional subbands as all k_j are real. However, due to the strong non-parabolicity of the bulk dispersion, the positions of the subband minima and the subband dispersions can only be found by solving (16) numerically.

IV. Subbands Dispersions

The dispersions of several electron and hole subbands is shown in Fig.5. The lowest electron/top most hole subbands display almost a linear dispersion. This distinguishes the subbands from those in silicon films. The energies of the subbands are lying in the bulk band gap (Fig.1). The subbands correspond to the topologically protected edge modes.

A close inspection demonstrates that a very small gap is opened at $k_x = 0$ reflecting the fact that the topological states located at the two opposite edges of the nanoribbon are not independently propagating and start interaction at small k_x[6]. At larger k_x the coupling between the edge states becomes insignificant as the edge states are moving in opposite directions and are located at opposite edges (Figs 3,4).

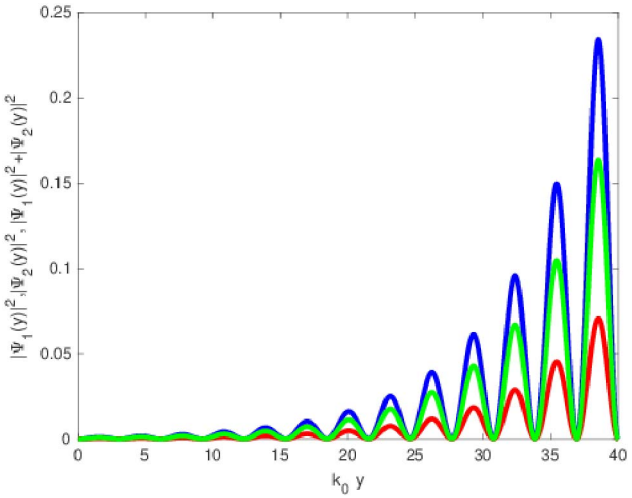

Fig.4 The same as in Fig.3, but for k_x =-0.1k_0. The wave function is for the state propagating in the opposte direction. It is localized at the oppoite edge.

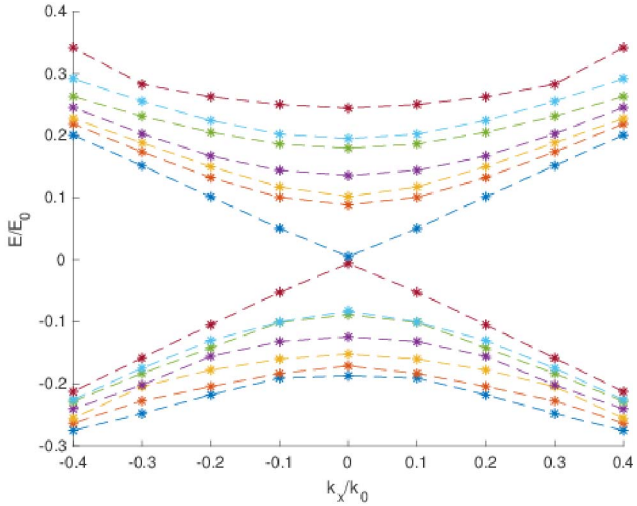

Fig.5 Subbands in a nanoribbon of the width d=40/k_0. E_z=0. The subband with an almost linear dispersion corresponding to the topologically protected edge state is clearly seen.

The gap between the bulk bands increases with the vertical electric field E_z. By increasing E_z the gap can be reduced, closed, and opened again as a direct gap at one of the minima, Fig.1. This leads to the gap between the lowest subbands opening (Figs 6,7), and the linear dispersion becomes quadratic close to the subband minimum. At the same time the edge mode delocalises from the edge as at least two of k_j become real, which leads to increased scattering and results in a reduced current.

V. Conclusion

We evaluated the subband structure in a nanoribbon of 1T'-MoS_2, a two-dimensional topological insulator by assuming an effective k·p Hamiltonian. We demonstrate that, without electric field, the lowest electron/top most hole subbands lie in the bulk band gap and display a linear dispersion. These subbands correspond to topologically protected edge modes. We show that a very small gap opens at $k_x = 0$ due to the interaction of the topological states located at the opposite edges of the nanoribbon.

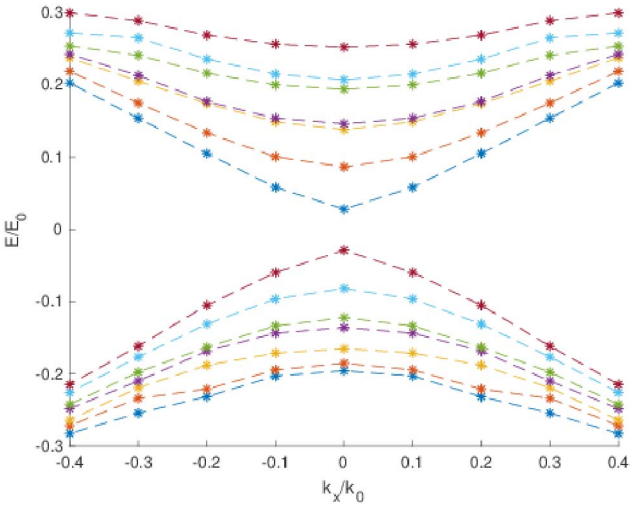

Fig.6 Subband energies at αE_z=$v_2 k_0$, when the gap at k_y=k_0 is closed, see Fig.1, red curve.

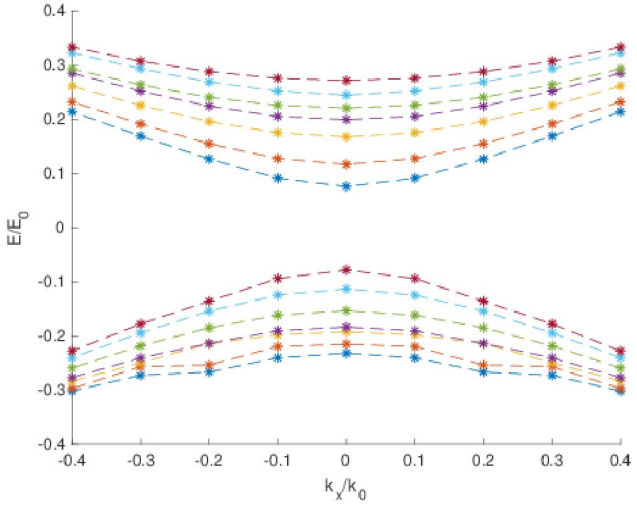

Fig.7 Subbands in a nanoribbon of the width d=40/k_0. at αE_z=$2v_2 k_0$ when the direct gap is opened again at k_y=k_0, see Fig.1, blue curve.

In contrast to the bulk case where the gap between the bands is reduced, closed, and opened again with the vertical electric field E_z, the gap between the edge modes never closes and always increases with the electric field. Together with the delocalization of edge modes with the electric field, the gap increase leads to the decrease of the nanoribbon conductance, which is promising for transistor applications.

Acknowledgment

Financial support by the Austrian Federal Ministry for Digital and Economic Affairs and the National Foundation for Research, Technology and Development is gratefully acknowledged. A.-M.B.E.-S. was supported in part by project No. IN 23/2018 'Atom-to-Circuit' modeling technique for exploration of Topological Insulator based ultra-low power electronics' by the Centre for International Cooperation & Mobility (ICM) of the Austrian Agency for International Cooperation in Education and Research (OeAD).

References

[1] L. Kou, Y. Ma, Z. Sun, T. Heine, and C. Chen,"Two-dimensional topological insulators: Progress and prospects", J.Phys.Chem.Lett. vol.8, pp.1905-1919, 2017.

[2] W.G.Vandenberghe and M. V. Fischetti, "Imperfect two-dimensional topological insulator field-effect transistors", Nature Communications, vol.8, art.14184 (pp. 1-8), 2017.

[3] Yu.Yu. Illarionov, A.G. Banshchikov, D.K. Polyushkin, S. Wachter, T. Knobloch, M. Thesberg, L. Mennel, M. Paur, M. Stöger-Pollach, A. Steiger-Thirsfeld, M.I. Vexler, M. Waltl, N.S. Sokolov, T. Mueller, and T. Grasser, "Ultrathin calcium fluoride insulators for two-dimensional field-effect transistors", Nature Electronics, vol.2, pp.230-235, 2019.

[4] X. Qian, J. Liu, L. Fu, and Ju Li., "Quantum spin Hall effect in two-dimensional transition metal dichalcogenides", Science, vol. 346, issue 6215, pp.1344-1347, 2014.

[5] L. Liu and J. Guo, "Assessment of performance potential of MoS_2-based topological insulator field-effect transistors", J.Appl.Phys., vol.118, art.124502 (pp.1-5), 2015.

[6] B. Zhou, H.-Z. Lu, R.-L. Chu, S.-Q. Shen, and Q. Niu, "Finite size effects on helical edge states in a quantum spin-Hall system" Phys.Rev.Lett., vol.101, art.246807 (pp.1-4), 2008.

[7] V. Sverdlov and S. Selberherr, "Silicon spintronics: Progress and challenges", Phys.Rep., vol.585, pp.1-40, 2015.